京都大学防災研究所年報 第 65 号 B
DPRI Annuals, No. 65 B, 2022

Investigation of Mechanisms Analysis in the Transition from Single-cell to Multicell Thunderstorms Using X-band Polarimetric Radar Observation

Fauziana AHMAD(1), Kosei YAMAGUCHI and Eiichi NAKAKITA

(1) Graduate School of Engineering, Kyoto University

Synopsis

The localized heavy rainfall induced by the single-cell could be more hazardous if the single-cell merged into the multicell thunderstorms. Flash floods and landslides are common disasters with a lifespan of multicell more than one hour and a scale of an area larger than a single-cell. To mitigate the flood risk, the short-term precipitation forecast is suggested as one of the observation tools to disseminate early warnings for the flood forecasting systems. Therefore, the study of the transition from single-cell to multicell was proposed by utilizing vertical vorticity. The mechanisms studied using dual-Doppler analysis (DDA) were further reviewed to quantify their relationships with vertical vorticity. The characteristics of single-cell could be characterized using vertical vorticity, where the formation height of the peak of core pair vorticity occurred at 4.4 km, and their peak of vortices developed at the same time of occurrence using pseudo-vorticity. Meanwhile, dual-Doppler vorticity analysis observed its formation height at 3.8 km and 3.7 km for positive and negative vorticity, respectively, which occurred in the same period. It was assumed that the period of peak intensity occurred at a similar time for single-cell, which was related to the initial formation of the updraft. The results of mechanisms analysis from the evolution of cell development were mainly affected on the increment of core vorticity intensity. The convergence, updraft, and stretching of the vortex tube were influenced on the increment of core vorticity intensity, especially at the lower level, and the tilting of the vortex tube was mostly affected at the middle-level height. At the later stage of multicell formation, the mature vortex was discovered with the core vorticity maxima boundary remaining due to the existence of updraft and convergence in the development of multicell.

Keywords: single-cell, multicell, updraft, convergence, stretching of vortex tube, tilting of vortex tube

1. Introduction

The localized heavy rainfall from cumulonimbus clouds commonly occurred in the summer season potential to be a hazardous cloud. In 2008, a flash flood occurred in the Toga River Basin located in Kobe, Japan due to the downpour of Guerilla-heavy rainfall from the development of isolated cumulonimbus clouds (Nakakita et al.,2013; Nakakita et al.,2017). The rapid rise of the water level in the river basin caused the death of five people. The dissemination of early warnings could not be delivered promptly since the flood came rapidly. Furthermore, the single-cell clouds could be merged into multicell clouds, which have a common lifetime of more than an hour and greater aerial

coverage than a single-cell. Small-to-medium-sized hail, small tornadoes, and heavy precipitation are all risks linked with multicell. Heavy precipitation from multicell thunderstorms also can intensify flash flood events, especially in urban areas. For example, the multicellular storm brought localized heavy rain near Zoshigaya, Tokyo on August 5, 2008, causing five sewage workers to be washed away by a flash flood (Kato and Maki 2009; Hirano and Maki 2010; Kim, et al. 2012).

Referred to the case of the Toga River basin, Nakakita et al, (2013, 2017) developed prediction methods on the first radar echo aloft that was described as a "baby-rain-cell" in a single cumulonimbus cloud using Doppler weather radar observation. According to the studies, the vertical vorticity values should be greater or equal to 0.03 s^{-1} to identify the hazardous rain cell in the initiation stage before it developed to the cumulus stage. This criterion is currently used in weather radar observation data of the XRAIN operated by MLIT to deliver early warnings to local governments. It focused only on the vertical vortex tube of a single-cell that connected at different altitudes and did not evolve into multicell development.

Rather than forecasting the detection of localized heavy rainfall, multicell formation studies in Japan are mostly investigated to understand the characteristics and its stage of formation. Previous research has focused on radar reflectivity (Nishiwaki et al., 2013; Shusse et al., 2005; Geng et al., 1997) based on the stage of multicell development. Kim et al. (2012) analyzed the precipitation core development and its structure by combining liquid water content (LWC) and K_{dp}. Consequently, the detection of hazardous clouds using short-term precipitation forecasts have been successfully developed in Japan to assist the forecasters to analyze the stages of cloud development and disseminate the early warnings to the public and flood warning system.

Many researchers analyzed the mechanisms that supported multicell development such as wind shear, convergence, updraft, and downdraft. These mechanisms are important to the stages of development of thunderstorm clouds. The vertical vorticity analysis is mostly investigated in supercell thunderstorms owing to the exhibition of updraft rotation. In addition, a vorticity pair in the baby-rain-cells was detected, which was related to the existence of an updraft in the single-cell. Therefore, the characteristics and mechanisms for the development from single-cell to multicell thunderstorms which are contributed to localized heavy rainfall motivated the author to discover the significant criteria related to the severity of thunderstorms. The quantification of the mechanisms that influence the interaction between cell merging in promoting the generation of strong heavy rainfall also contributes to the enhancement of knowledge in the transition process from single-cell to multicell development.

2. Data and methodology

2.1 DDA vorticity analysis

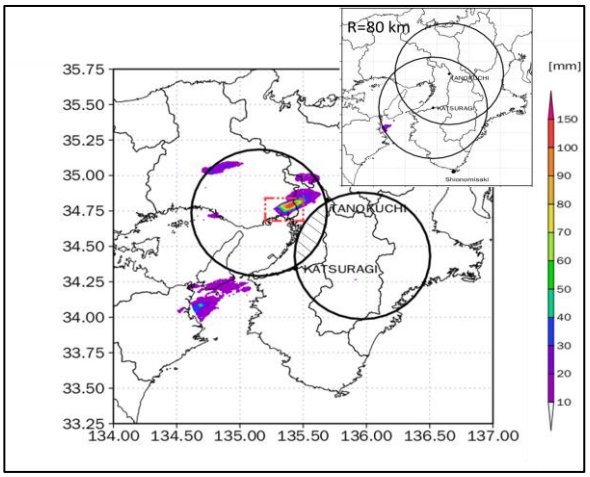

Fig. 1 Two Doppler radars at Tanokuchi and Katsuragi cover a radius of 80 km (the full observation domain is shown in a box at the upper-right corner. Dual Doppler radar map used for the target area (red box color) was conducted within two solid circles except for the hatched area.

The core vorticity of the DDA was defined as the maximum intensity of the positive vorticity and the minimum intensity of the negative vorticity intensity, which was obtained for each CAPPI height. In the DDA vorticity estimation, two Doppler radars namely Tanokuchi and Katsuragi radar stations were used as presented in Fig.1. The spatial and temporal resolutions of this analysis were 1 km × 1 km × 0.5 km and 5 min intervals, respectively.

The illustration of the estimation of DDA vorticity is shown in Fig.2. In the Cartesian coordinate system, the vertical vorticity is expressed as Equation (1):

$$\zeta = \frac{\partial v}{\partial x} - \frac{\partial u}{\partial y} \qquad (1)$$

where u is the zonal wind component, and v is the meridional wind component in the x and y direction, respectively.

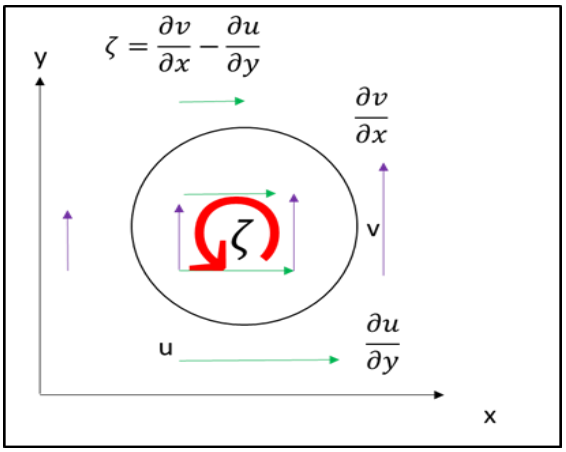

Fig.2 Schematic illustration of DDA vertical vorticity analysis.

The classification of the single-cells was determined with a closed contour of Z_h > 10 dBZ at a height of 2 km. The multicell was defined when more than one core of Z_h > 10 dBZ at the height of 2 km was observed. The merging of the echoes between the single-cell and multicell could be determined by monitoring the edge of the contour line of > 10 dBZ echoes at a height of 2 km and the increase in Z_h 5 min after merging. The maximum values of the positive and negative vorticities were identified to calculate the core vorticity at each cell boundary. The locations of the positive and negative core vorticities were ensured to be consistent so that the vertical vortex tube could be constructed.

2.2 Pseudo-vorticity analysis

The pseudo-vorticity is observed at a single radar, and the selection of radar is dependent on the distance from the radar to the target area. The selection also considers the data is not affected by radar noise errors such as blockage and data contamination. For the extraction of vorticity distribution from Doppler velocity, it was converted directly from raw data in the polar coordinate system without interpolation to analyze the vortex tube analysis.

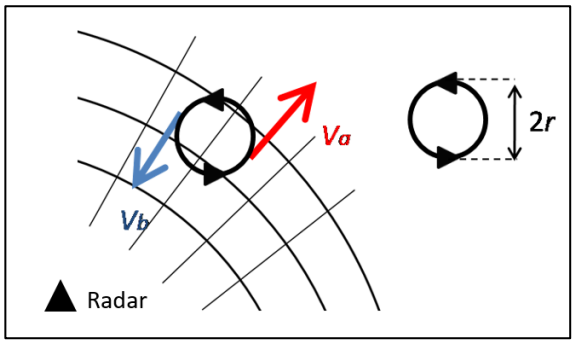

Fig.3 Illustration of pseudo-vorticity estimation using single radar.

The pseudo-vorticity was estimated by applying the method proposed in Nakakita et al. (2017) with a spatial resolution of 50 m × 50 m in each elevation angle at 1 min intervals. Using the radial velocity speed, the vorticity can be calculated by using Equation (2),

$$\zeta = 2 \times \frac{V_a - V_b}{2r} \qquad (2)$$

where V_a and V_b are the radial velocities moving toward and away from the radar in the Cartesian coordinates, respectively, and 2r is the total distance of radar pulse between the mesh's center. The illustration of pseudo-vorticity estimation is illustrated in Fig.3.

In this study, the core vorticity is defined as the maximum intensity of the positive and negative vorticities at each plan position indicator (PPI), which was extracted from the 1-min data for each elevation angle of PPI. In addition, the moving average method (150 m and 550 m) was used in this study for more enhancement of the vertical vorticity structure.

2.3 Characteristics patterns

The characteristic patterns of transition from single-cell to multicell in the multicell thunderstorm environment were determined by examining the intensity, and height of each core vorticity. We

focused on the inspection of the peak intensity during the analysis period with respect to height and time. For the pseudo-vorticity, the height of cells developed was calculated using Equation (3), by considering the height of the center of the radar beam h is given at a distance r by the equation adapted from Rinehart (2010).

$$h = \left[\sqrt{r^2 + (k_e a)^2 + 2r\,(k_e a + H_0)\,sin(\theta_e)}\right] - k_e a \quad (3)$$

where a is the earth's radius, k_e is the ratio between a and the equivalent earth's radius, θ_e is the antenna elevation angle, and r is the distance between from radar to the point of target, and H_0 is the height of the radar above sea level. In this study, k_e was assumed as the standard refraction with the value of k_e is approximately 1.3333.

A schematic illustration of the height determination is displayed in Fig.4 for the pseudo-vorticity analysis. The height of DDA vorticity could be retrieved based on the CAPPI height formation.

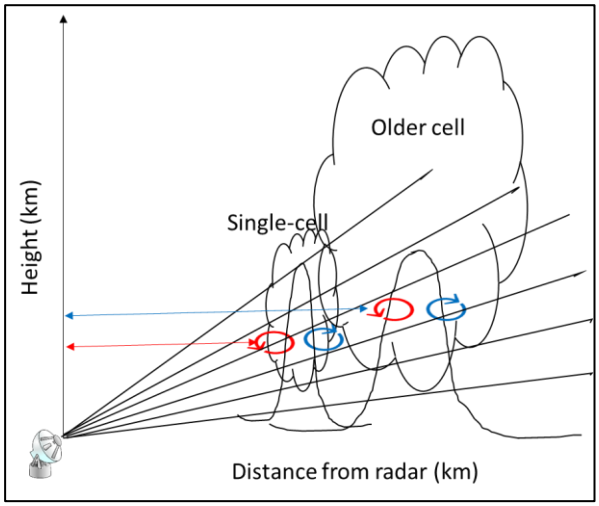

Fig.4 Schematic illustration of height calculation from the pseudo-vorticity analysis. The red anticlockwise arrow indicates positive vorticity; the blue clockwise arrow specifies negative vorticity.

2.4 Mechanisms analysis

It has been discovered in numerous studies that tilting and stretching mechanisms are required for the dynamic formation of vorticity (Rotunno, 1981; Shapiro and Kogan, 1994; Boyer and Dhal, 2020), especially for supercell. Therefore, both mechanisms will be further investigated to analyze the vortex tube structure associated with the single-cell merged into multicell.

The rate of change in the vertical vorticity can be described by Equation (4), where the first and second terms on the right side of the equation represent the tilting of the horizontal vorticity and the third term represents the stretching of the vortex tube.

$$\frac{d\zeta}{dt} = \xi\frac{\partial w}{\partial x} + \eta\frac{\partial w}{\partial y} + \zeta\frac{\partial w}{\partial z} \quad (4)$$

where (ξ, η, ζ) are vorticities in the (x,y,z) direction, respectively, and w is the z-component of velocity.

The tilting term is important for the mesoscale process such as tornadoes which tilt the horizontal vorticity to vertical vorticity. The stretching term exponentially increases the vertical vorticity that is co-located with the horizontal convergence of air. The convergence in the updraft and the divergence in the downdraft affect the vortex pair intensity at the lower and middle levels (Rotunno, 1981). Therefore, both factors will be examined in this study. Divergence as a property of the flow field is shown in Equation (5). Negative divergence is convergence in this study.

$$\text{Divergence} = \frac{\partial u}{\partial x} + \frac{\partial v}{\partial y} \quad (5)$$

where u is the zonal wind component, and v is the meridional wind component in the x and y direction, respectively. These equations (4) and (5) use the wind fields obtained by dual-Doppler analysis at 5-minute intervals.

3. Environmental conditions

In this study, we observed the storm cluster in the Kinki region and chose only events with heavy precipitation that occurred due to the atmospheric instability with the condition of multicell formation. The environmental condition of instability condition can be evaluated using Convective Available Potential Energy (CAPE) and Bulk Richardson Number (BRN) using radiosonde data observation.

The low value of CAPE is not sufficient to support the multicell formation. According to a study, a typical multicell (or supercell) environment over the Great Plains (e.g., 2022 J kg^{-1} for a multicell, Stalker and Knupp 2022; 2542 J kg^{-1} for an Oklahoma supercell, Bluestein and Jain 1985). However, the frequency distribution of CAPE in the Tokyo region has been recorded at a value of 1000 J kg^{-1} at Tateno, in May between 1990 and 1999 (Shimizu et al., 2008). In general, BRN > 45 is favorable for multicell formation from a study (Weisman and Klemp 1982, 1984, 1986; Peterson 1984; Bluestein and Jain 1985). We will consider these two types of atmospheric instability indicators as well as the environmental condition derived from the JMA Mesoscale Model (MSM).

This study focused on the broken areal-type formation related to the development of an unstructured area relative to moderate-to-intense cells that merged into a line of convective storms. According to Bluestein and Jain (1985), this type of multicell has a longevity of 30–90 min without repetition, with the cluster storm. The nearly $2^{1/2}$ hours of observation showed the maximum accumulated rainfall was 150 mm. There was a report of a flood that occurred in Ikeda city due to a downpour of heavy rainfall that reach 100 mm for one hour.

The observed atmosphere in this region was sufficiently unstable for multicell formation. Relative humidity (RH) at 1000hPa and the surface wind vectors (Fig. 5(a)) were obtained from the JMA MSM. RH in Kinki region was > 80% and over the ocean to the north was > 90%, while the ocean surface temperature was >26℃. The surface weather map presented the confluence on the target area and indicated the rising motion. Consequently, warm and humid air flowed towards the observation areas from the ocean south of Osaka bay. CAPE and vertical shear values from the surface to 6 km (866 J/kg and 0.003 s^{-1}, respectively) were calculated based on data observed at the Shionomisaki Station, approximately 150 km away from the target area at 2100 JST. BRN was calculated to be 60, indicating a multicell similar to the storm type classification. However, the event was locally affected by southwesterly winds from Osaka Bay, as shown in Fig. 5(b).

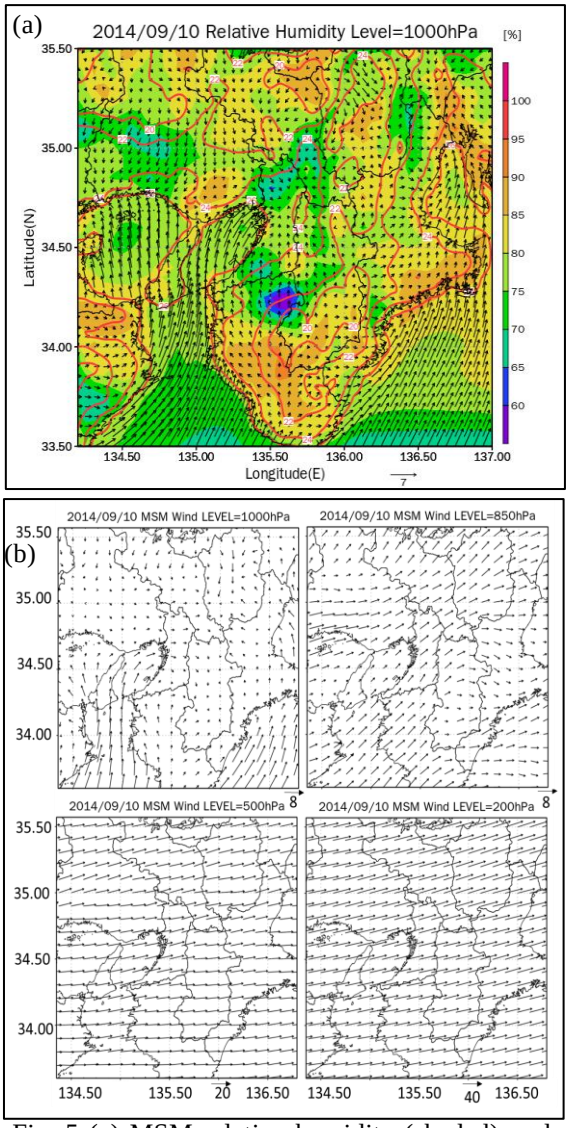

Fig. 5 (a) MSM relative humidity (shaded), red contour (surface temperature) (b) MSM wind level analysis. Images are based on data obtained on 10 September 2014.

4. Results and discussions

The transition from single-cell to multicell with the vertical cross-section through the storm will be explained in this section.

The evolution of multicell formation is illustrated in Fig. 6, which presents the horizontal section of radar echoes and wind motion at altitudes of 2 km at 5-minute intervals. Apparently, this cluster storm was a multicell thunderstorm that composed several cores of radar reflectivity in almost 2-hour observation. The storm propagated from the southeast to the northeast which started from a single-cell and combined with other cells that

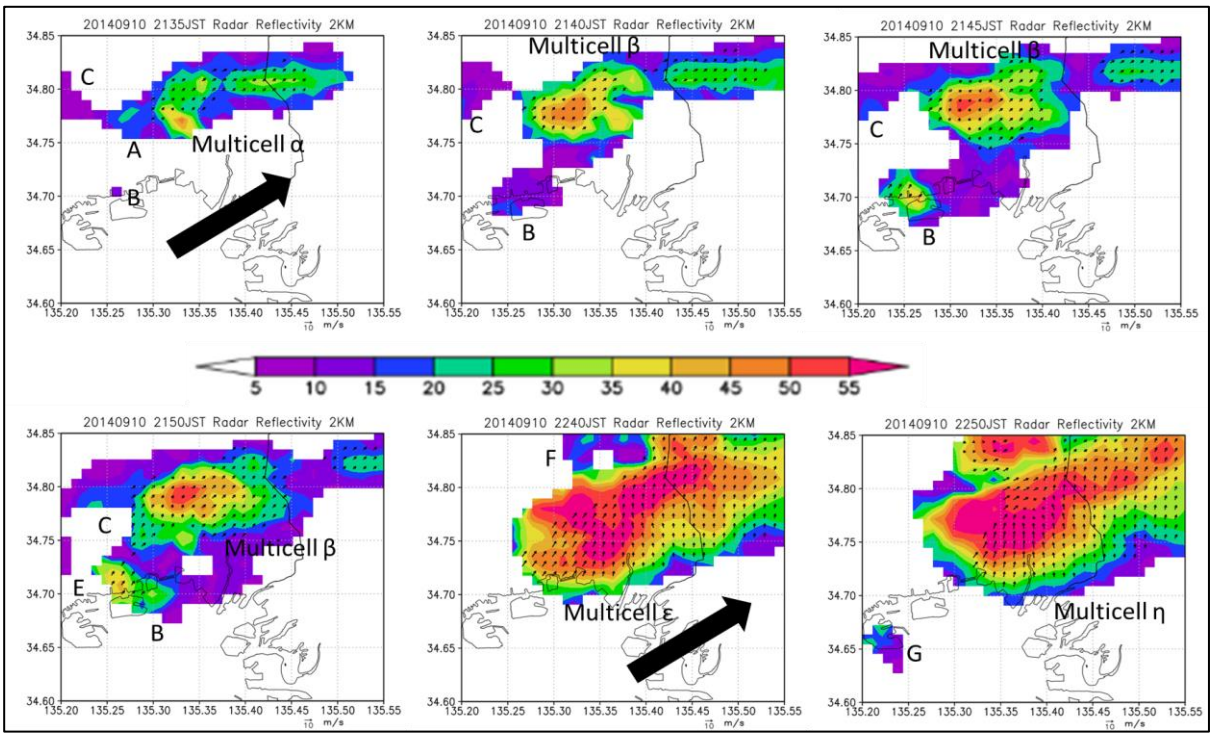

Fig.6 Storm propagation including the labels of the single-cells and multicell at a height of 2 km above the ground level. The black arrow indicates the storm motion movement.

were newly generated at the left flank (relative to the direction of the cell motion) of the storm, and parent cells decayed on the right flank. The lifetime of the storm was more than 2 hours. It is noted that cell A developed very strongly at 2150JST. The multicell ε and η then developed with the strongest intensity and expanded in the large area.

Shown in Fig.7 are the changes with time of maximum radar reflectivity, vertical vorticity, and updraft velocities within the storm. During the one-hour observation, maximum reflectivity was increased from 30 dBZ to 50 dBZ and, it gradually rose until 70 dBZ. The maximum updraft speed increased from <1.5 ms^{-1} to >5 ms^{-1}, and rapidly increased after 1-hour observation. The peak of vertical vorticity occurred at the early development of multicell, then gradually increased after 2200JST. The rapid increment could be observed on the peak vorticity at 4 km height compared with 2 km AGL. Mostly the peak of updraft was consistent with the peak of vertical vorticity. These changes indicate the storm gradually developed with the merged of single-cell and adjacent cells, therefore, a detailed investigation in terms of vertical vorticity and kinematic mechanism will be investigated.

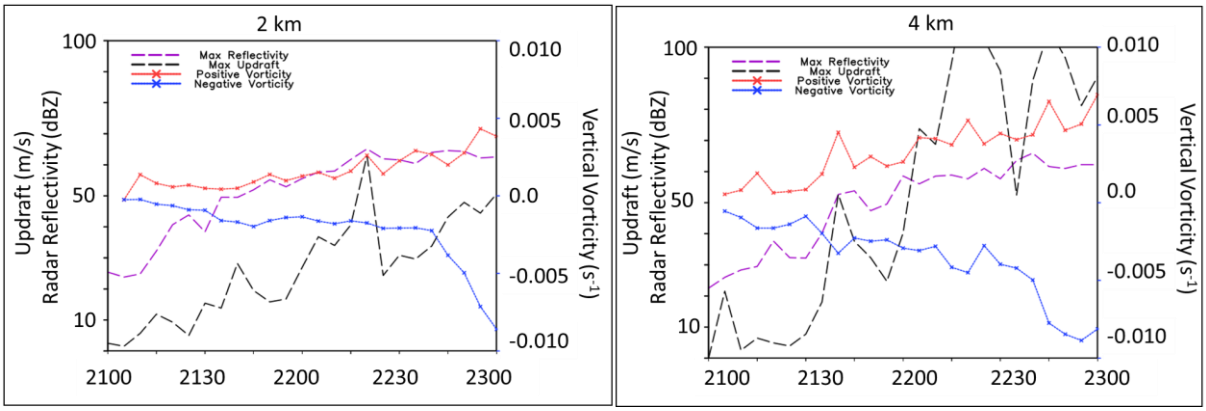

Fig.7 Core vorticity, maximum reflectivity, and updraft during the entire storm at 2 km and 4 km. The circle indicated the peak of vorticity that happened in the multicell development.

4.1 Characteristics and mechanisms analysis

In the pseudo-vorticity analysis, at the early stage of multicell formation, it was found that single-cell A indicated the greatest intensity of vertical vorticity compared with multicell α after the merging occurrence at time 2134JST. The core vorticity of boundary cell A rapidly increased after the merging at 2134 JST, and the intensity of the core vorticity peaked at 2137 JST, that was, 3 min after the merging. The maximum intensities of cell A were 0.076 s^{-1} and –0.110 s^{-1}. The intensity of the core vorticity of cell α did not rapidly increase after merging. The maximum values (0.023 s^{-1}, –0.02 s^{-1}) could be observed at 2131 JST.

Meanwhile, single-cell E indicated less intensity compared with multicell ε during the 10-minute observation. After merging, there was a rapid increase and sudden decrease of the multicell, then remained steady at the end of the analysis. The maximum intensities of cell E were 0.036 s^{-1} and –0.037 s^{-1} at 2243JST. The intensity of the core vorticity of cell ε rapidly increased after merging. The maximum values (0.069 s^{-1}, –0.070 s^{-1}) could be detected at 2243 JST. Other single-cell B, D, and F showed a pattern similar to the single-cell E, in which the intensity of multicell was higher than single-cells. However, in the time-series analysis, the peak of core vorticity was mostly observed for both cells. Therefore, the peak of core vorticity is indicated as the transition signals of vertical vorticity that merged into the multicell. Later, these transition signals will be analyzed in conjunction with their formation height.

The peak intensity of core vorticity of the cells investigated is summarized in this section for DDA analysis. Based on the early formation of multicell from 2100 to 2200 JST, multicell (α, β, γ, δ) indicated the persistence of the core vorticity intensity (0.003 s^{-1} and –0.003 s^{-1}). The core vorticity of cells B, C, and D ranges from 0.003 to –0.002 s^{-1}. At the latter stage of multicell formation, the intensity of the core vorticity of the multicell increased after it merged with the single-cells E and F. The positive and negative vorticities range from

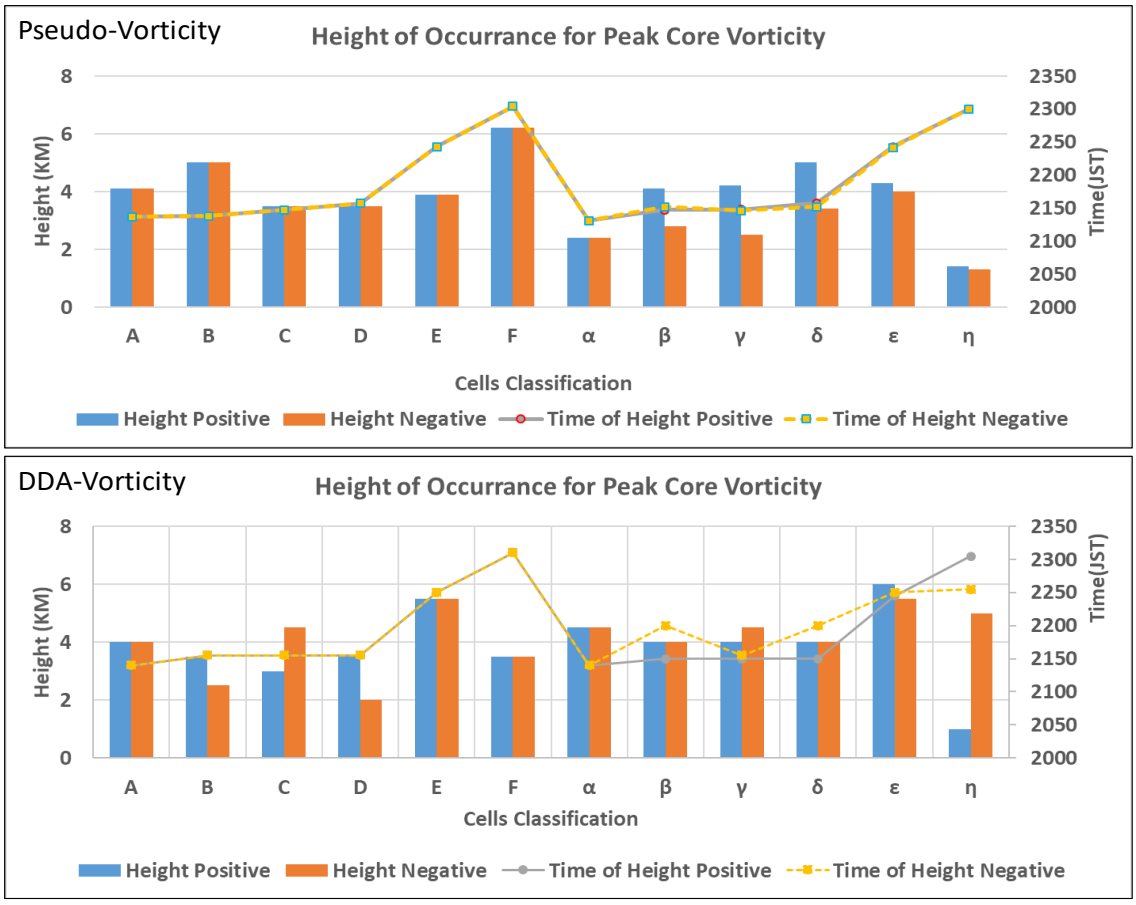

Fig.8 The time investigation of formation height and time occurrence of peak core vorticity

0.008 to 0.009 s^{-1} and from –0.010 to –0.012 s^{-1}, respectively, revealing the core vorticity maxima of the multicell. The intensities of the core vorticity of cells E and F are 0.005 and –0.012 s^{-1} and 0.004 and –0.004 s^{-1}, respectively. All single-cells that merged with the multicell showed lower core vorticity, except for cells A, E, and F. These characteristic patterns revealed similarities with the pseudo-vorticity analysis method.

As shown in Fig.8, the pseudo-vorticity method could distinguish the height of peak core vorticity between single-cell and multicell. The height of peak core vorticity of positive and negative for single-cells showed a similar height approximately in the range of 3 to 4 km except for cell F. In contrast, the height of peak core vorticity was discovered at various heights which the height of the multicell showed in the range of 2-6 km AGL. The average formation height of single-cell was 4.4 km for both pair core vorticities. In contrast, multicell showed the average formation height was 3.6 km for core positive vorticity and 2.7 km for core negative vorticity.

In the DDA vorticity method, the height of peak core vorticity was observed at a similar height for single-cells A, E, and F, together with multicell α, β, and δ, in the range of 4 to 6 km. There was various height of peak core vorticity that were observed in the single-cell and multicell. The average formation height of single-cell was 3.8 km and 3.7 km for core positive and negative vorticity, respectively. In contrast, the average formation height for multicell was 3.9 km for core positive vorticity and 4.6 km for core negative vorticity. The calculated average formation height for the maximum updraft for single-cell and multicell were 3.9 km, and 4.0 km, respectively. These patterns of formation height of updraft are similar to the height of core vorticity from the DDA method. Thus, the relationship between the height of peak core vorticity intensity and maximum updraft existed in this study.

In terms of the occurrence time of peak core vorticity, the pseudo-vorticity method presented the equivalent period of peak intensity. We could conclude that the pseudo-vorticity can differentiate the characteristics of single-cell and multicell in terms of height and developing time of peak core vorticity intensity due to the high spatial and temporal resolution of estimation. In terms of occurrence time of peak core vorticity, this method revealed a similar period of the developed peak at single-cell only, but not in the multicell. These characteristic patterns are dissimilar to the pseudo-vorticity method. DDA vorticity is not capable to

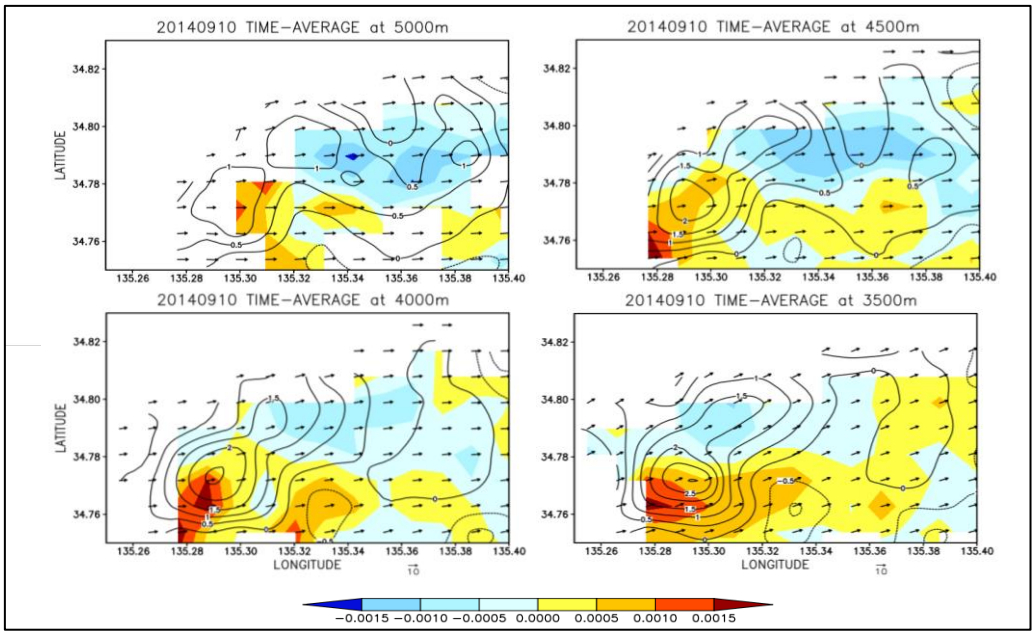

Fig.9 The spatial changes of vertical vorticity from 3.5 km to 5.0 km with positive vorticity(red color), and negative vorticity (blue color) shaded region. The solid black contour indicated updraft with an interval of 0.5 m s^{-1}. The dashed black contour specified the downdraft.

distinguish the pattern of single-cell and multicell owing to the low temporal and spatial resolution. However, we assumed that the peak of core pair vorticity in the single-cell developed at the same period due to the updraft development, meanwhile, in the multicell, it presented the different occurrence peak of pair vorticity due to the updraft and downdraft influenced in the multicell.

As described in Fig.9, the time-average of single-cell developed into multicell, which occurred from 2120JST until 2130JST involving single-cells A, B, C, and D, revealed that the vertical vortex tube with the highest positive vorticity magnitude remained happened at the longitude of 135.28°E from 3.5 km until 4.5 km. It was also found that the maximum updraft was positioned adjacent to the position of maximum positive vorticity, and occurred at a similar time at each height. The location of maximum updraft was also identified as located adjacent to the core of positive vorticity, which concluded that the pair of vorticity existed in the multicell development similar to the supercell formation. The magnitude of rotation for multicell was found less than supercell which supercell mainly observed at the highest magnitude of positive vorticity at 0.1 s^{-1}, compared with the multicell attained at 0.005 s^{-1} in this study.

From Fig. 10(a), maximum updraft greater than 5 m/s in single-cell showed the dominant height from 3 km until 4.5 km, which the most frequently occurred at level 4 km. The position of the maximum updraft is almost identical to the average formation height of single-cell for core vorticity as analyzed in Table 4.3. Meanwhile, the maximum updraft as presented in Fig. 10(b) was greater than 5 m/s located between 3 km and 5.5 km, and the most frequent height was located at 4 km height. In addition, the maximum downdraft greater than -1 m/s, revealed the height was positioned at 1 km height, but the maximum downdraft still occurred until 5.5 km height, as illustrated in Fig. 10(c). From these analyses, we could have confirmed that the peak of vertical vorticity is correlated with the position of maximum updraft for single-cell, and updraft-downdraft in the multicell.

The time-series analysis showed similar transition patterns for single-cell and multicell with the increment intensity after merging for both

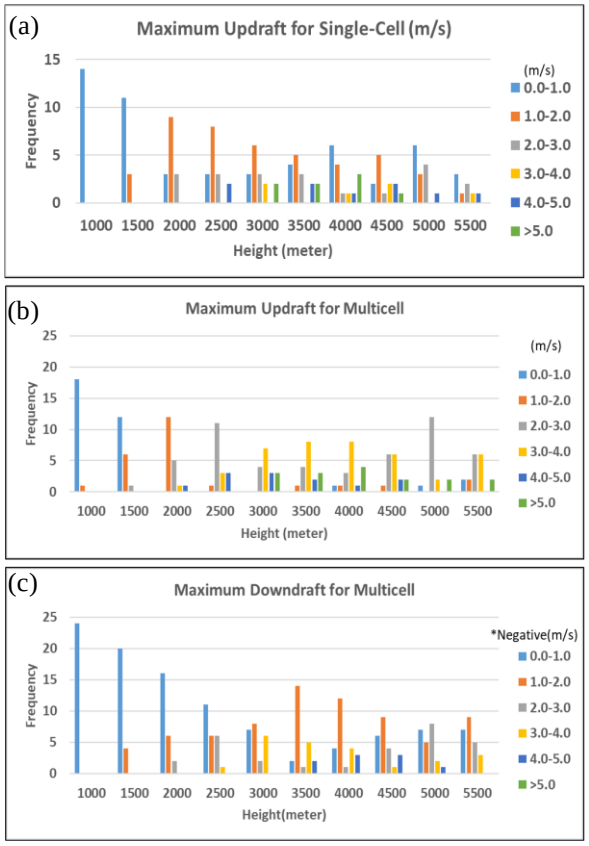

Fig.10 Distribution of maximum updraft for each height for (a) single-cell (b) multicell, and (c) distribution of maximum downdraft in multicell.

pseudo-vorticity and DDA vorticity methods at the early stage and later stage of multicell development respectively. As a result, in this section, we will show the analysis of single-cell A-multicell α, and single-cell F-multicell η for further discussion in terms of kinematic and dynamic analysis.

At the horizontal distribution of updraft and DDA vorticity, as shown in Fig. 11, the core of the updraft is located between the pair vorticity at the boundary of cells A and α at 2135JST. This result is similar to the findings of Franklin et al. (2006), which identified that the core of the updraft is located between the pair vorticity. Single-cell A specified the peak intensity of the updraft compared with multicell α at a height of 2.5 km, at 2140 JST.

Fig. 12(a) and Fig.12(b) present the vertical cross-section along the lines shown in Fig.11. In the W1-W2 section, at 2135JST, the single-cell A was developed at the middle level (2 km – 4 km) with the maximum updraft of 2.13 ms^{-1} at 3 km height. The inflow could be observed at the left flank of the

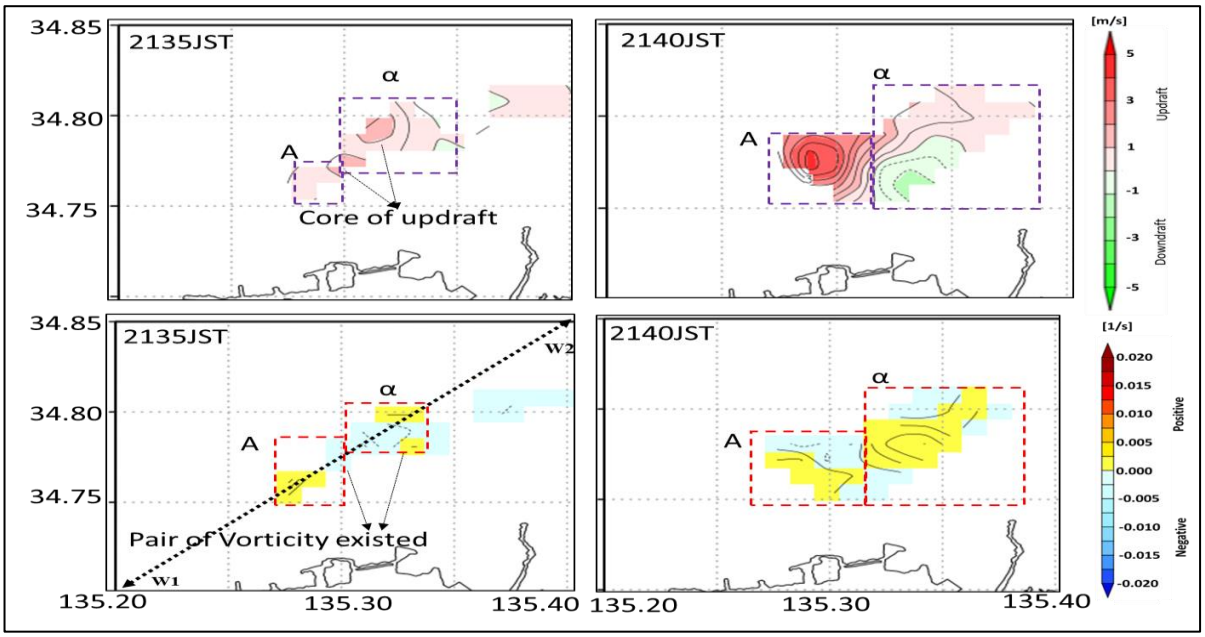

Fig.11 The horizontal distribution of updraft (top figure) and vertical vorticity (below figure) at 2 km height CAPPI.

downdraft (LFD) of the storm typically generated at this middle level. At this period, the maximum downdraft at the multicell developed at the lower level with the maximum intensity of 0.35 ms^{-1} at 2 km AGL. The single-cell A that was developed adjacent to multicell α, was influenced by the downdraft of the parent cell. With the existence of warm and moist inflow from the environment at the lower level and the convergence at the lower level, the updraft was generated at the boundary of cell A. The pair vorticity was discovered that developed at the middle-level height.

After 5-min observation (2140JST), the Z_h intensity of single-cell A increased, with the increment of convergence, updraft, and vertical vorticity during the cell merging development. The multicell α was observed at the lowest intensity, and single-cell A become more dominant at this time. The vertical vortex tube of single-cell presented a pair of peak vortices at the middle height, meanwhile multicell showed the pair of vorticity at the upper-level. The convergence intensity slightly increased with the updraft strength resulting in the dominance of single-cell A. In comparison, the divergence at the lower level indicated the descending air motion of multicell α to dissipate. These mechanisms proved that convergence and updraft are important mechanisms for the intensification and maintenance of core vorticity. The single-cell A currently showed the core of Z_h at 48 dBZ at 4 km height.

After cells merged at 2145JST, we could observe the widening areas of all mechanisms investigated whilst the core of Z_h (>40 dBZ) was observed near the ground. Therefore, the downpour of rainfall is mostly expected during this time in this area. It was found that another inflow started to develop at 4 km height yield to the advection of position for vortex tube in single-cell A. The convergence at the lower level and updraft remained happened in single-cell, but not in the multicell.

To evaluate the dynamic mechanism of vertical vorticity, the vertical cross-section through both cells is presented in Fig. 13(a) for stretching of the vortex tube and Fig. 13(b) for tilting of the vortex tube. We observed that the stretched vortex tube remained happened at the middle-level height which intensified the core vorticity in single-cell A. The tilting of the vortex tube produced a similar pattern of height, with the change in sign from left to right indicating that the tilting of horizontal vorticity associated with the gradient of vertical vorticity produces a couplet of counterrotating vortices that crossed the updraft.

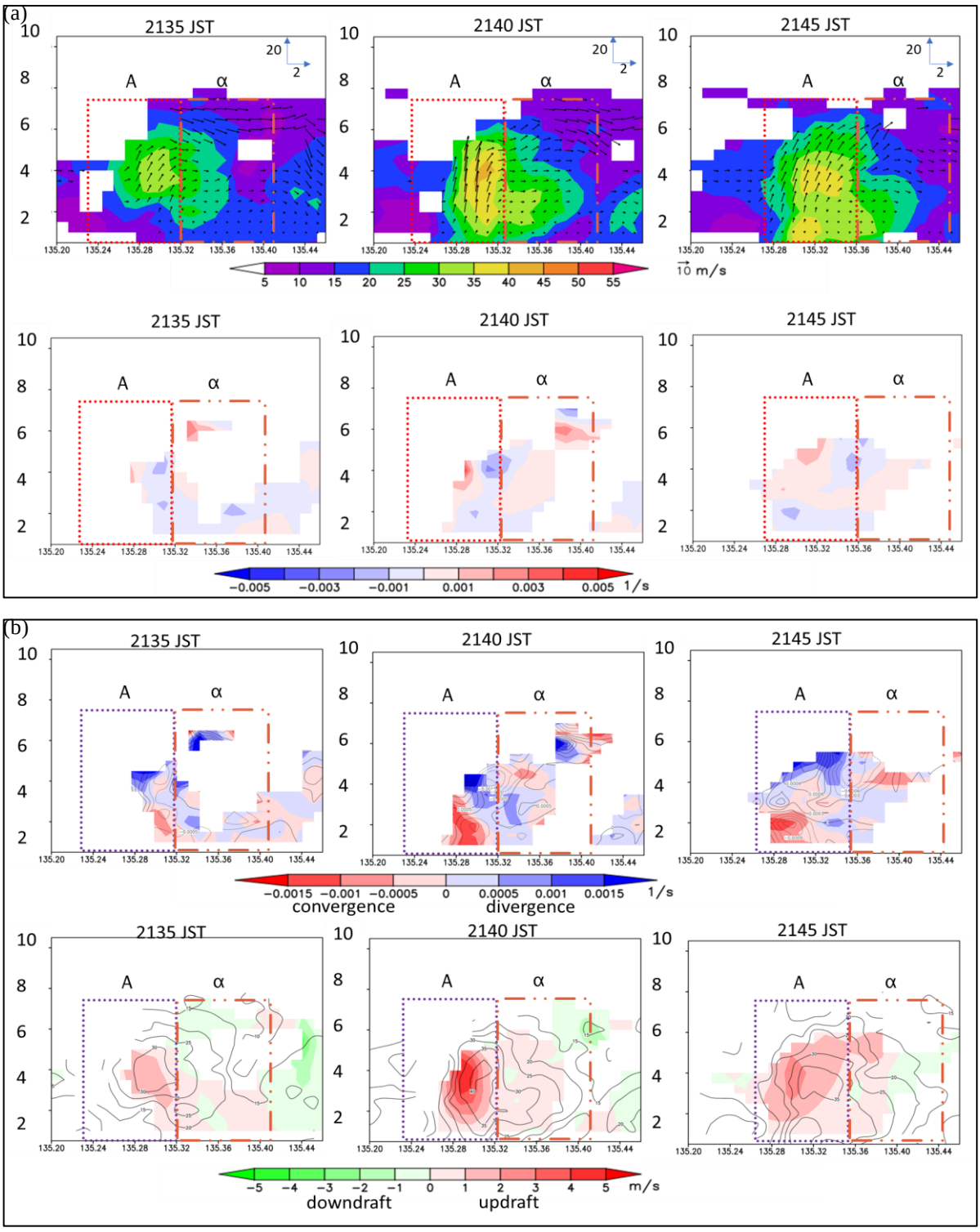

Fig.12 Kinematic analysis of cell A and multicell α. (a) Top figure indicates radar reflectivity with wind vector, below figure shows vertical vorticity. (b) Top figure indicates convergence (red color), and divergence (blue color), below figure shows updraft (red shaded color) and downdraft (green shaded color). See Fig.11 for the cross-line.

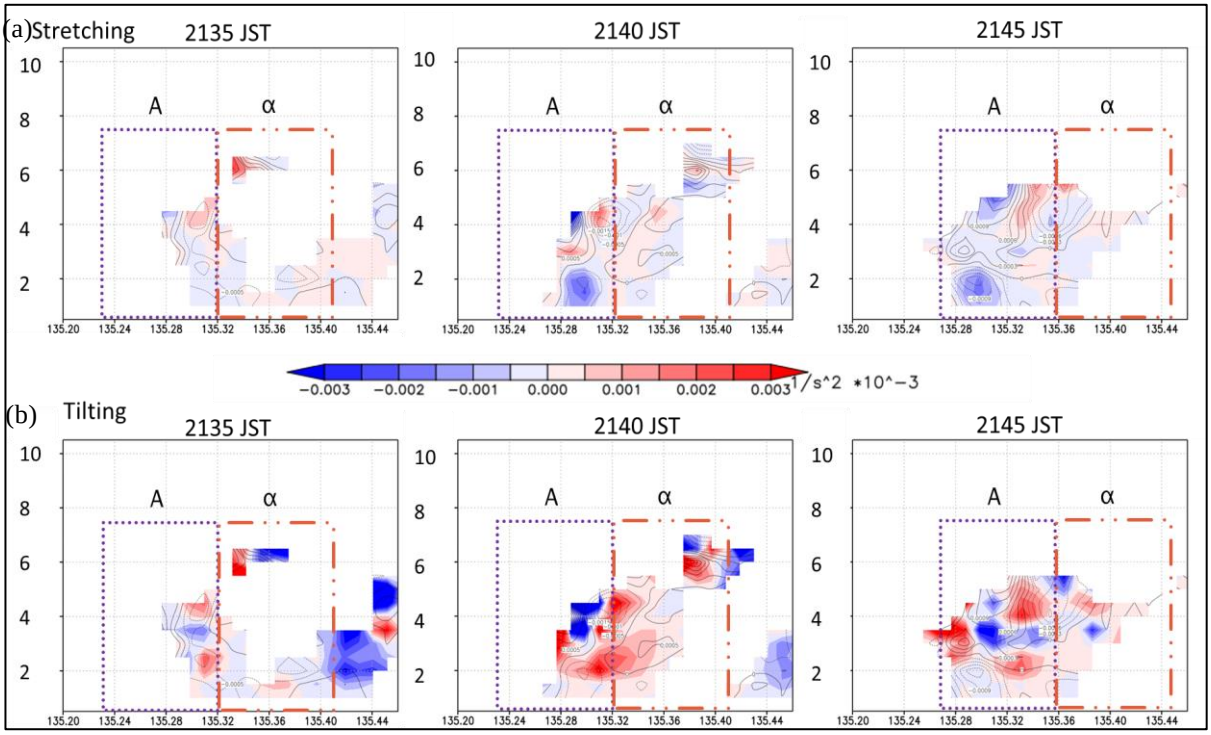

Fig.13 Dynamic analysis of cell A and multicell α. (a) Top figure indicates stretching term (b) below figure shows the tilting term.

At the horizontal distribution as presented in Fig. 14, the maximum updraft remained high intensity at the center of the storm at 2300JST and 2305JST. The downdraft was observed at the rear flank of the storm, and single-cell F propagated northeastward to merge with the existing multicell. The vertical vorticity was also located at the center of the updraft with the positive vorticity on the right and negative vorticity on the left flank of the storm.

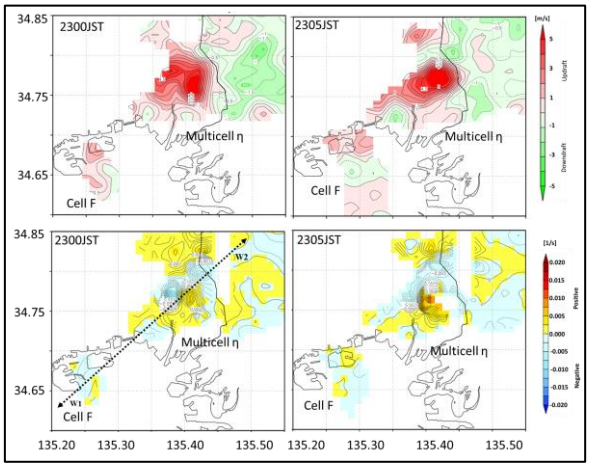

Fig.14 The horizontal distribution of updraft (top figure) and vertical vorticity (below figure) at 2 km height CAPPI.

Fig. 15(a) and Fig.15(b) present the vertical cross-section along the lines shown in Fig. 14. In the W1-W2 section, at 2255JST, the cell F was developed at a longer distance and started to merge with the existing multicell with the inflow could be observed at the left flank of downdraft (LFD) at the middle level (2 km–4 km) with the maximum updraft 3.03 ms^{-1} at 4.5 km height. During this period, the maximum downdraft at the multicell steadily developed with a maximum intensity of 4.72 ms^{-1} at 3.5 km AGL. The single-cell F that was developed far from the existing cell, was not influenced by the downdraft of the parent cell. However, with the existence of wind shear from the environment at the lower level, this cell merged and combined into one multicell. We discovered that the intensity of convergence at the lower level was small, the vertical vorticity showed the lowest intensity compared with the multicell. The pair vorticity in the vertical vortex tube was discovered that developed until the middle-level height.

After 5-min observation (2300JST), the Z_h intensity of cell A increased, with the increment of convergence, updraft, and vertical vorticity during the cell merging development. The vertical vorticity

of single-cell presented at the middle height, meanwhile multicell showed the pair of vorticity at a low level. The results indicate that the position of updraft and downdraft influence the location of pair vorticity after merging. The multicell always showed the core of Z_h at 45 dBZ at 2-4 km height. After cells merged at 2305JST, we could observe the widening areas of all mechanisms investigated whilst the core of Z_h was observed near to the ground, and single-cell merged observed the widening area of the core of Z_h at more than58 dBZ. Therefore, at this latter stage of multicell formation, the downpour of rainfall occurred near the ground, and with the merged of singe-cell, the intensity increased and covered more areas.

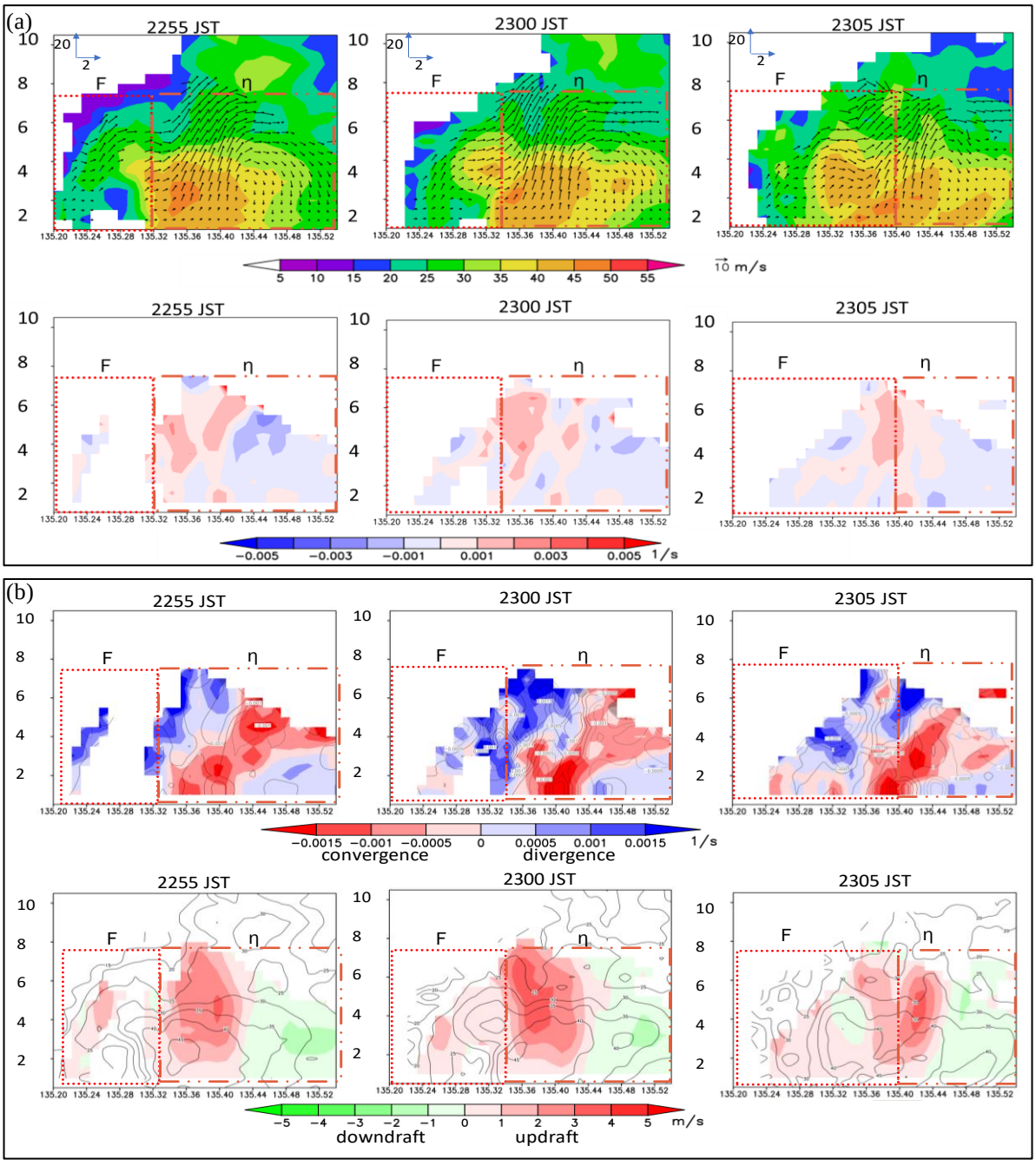

Fig.15 Kinematic analysis of cell F and multicell η. (a) Top figure indicates radar reflectivity with wind vector, below figure shows vertical vorticity. (b) Top figure indicates convergence (red color), and divergence (blue color), below figure shows updraft (red shaded color) and downdraft (green shaded color). See Fig.14 for the cross-line.

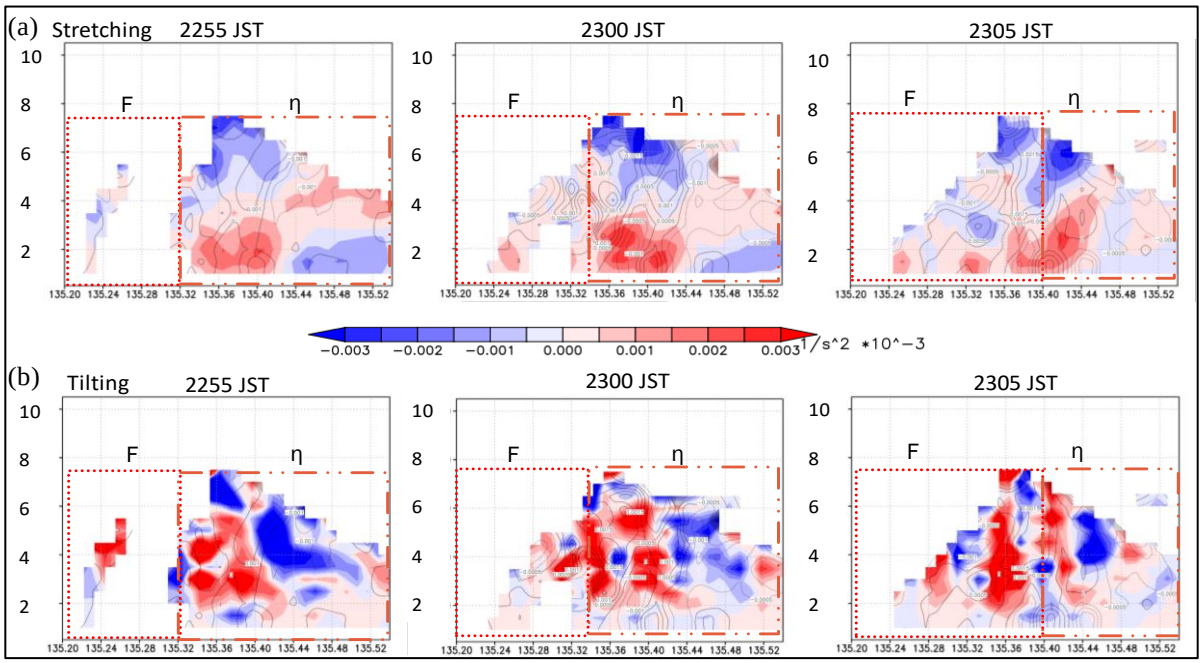

Fig.16 Dynamic analysis of cell F and multicell η. (a) Top figure indicates stretching term (b) below figure shows the tilting term.

To evaluate the dynamic mechanism of vertical vorticity, the vertical cross-section through both cells is presented in Fig. 16(a) for stretching the vortex tube and Fig. 16(b) for tilting of the vortex tube. We observed that the stretched vortex tube was influenced by the convergence at the lower level, and it remained happened at the multicell boundary, resulting in the increment of vertical vorticity intensity in the multicell compared with single-cell. The tilting of the vortex tube also provided the intense value at the middle height indicating the vertical wind shear that remained happened during the multicell storm.

From both analyses of single-cells A and F, the increment of core vorticity mainly happened because of the merger of two cores with different ages, in which the single-cell specified the developing stage, meanwhile the multicell showed the maturing or dissipating stage. Although the vertical vorticity was indicated upon 5-minutes after cells merged, the peak of core vorticity indicated the transition of single-cell to multicell.

The mechanisms that amplify the intensity of vertical vorticity were mainly studied and agreed that low-level convergence is the primary mechanism in vertical vorticity (Shapiro et al., 1999; Markowshi and Hannon, 2006; Dahl et al., 2017). The stretching term is composed of the divergence term and the vertical vorticity. Furthermore, the increment of core vorticity from time to time might be influenced by the tilting term. The horizontal vortex tube will be tilted to the vertical vortex tube with the sign of pair vorticity depending on the environmental wind shear.

A previous study by Rotunno (1981) showed that in a thunderstorm, a pair of clockwise-anticlockwise vorticity is generated by tilting of the horizontal vortex. Nakakita et al (2017) utilized this pair of vorticity to identify hazard rain cells before they were generated into a single thunderstorm. Both studies did not discuss about the pair of vorticity during the transition from single into multicell.

In the vortices merger, the local change of vertical vorticity could be influenced by the stretching and tilting of vortex tube in the transition from single-cell to multicell and inside the multicell too needed to be understood. Therefore, in this study, we found that low-level convergence influenced in the stretched of the vortex tube during the merged cells. From this analysis of vortices merger, we could see the increment of core vorticity due to the existence of convergence that stretched the vortex tube. Two vortices at the same sign (orientation) with (almost) parallel axes, within a certain distance, mix (merge) a substantial portion of their core vorticity into a single vortex (P.Meunier et al., 2005).

5. Conclusions

A dual-Doppler processing is beneficial in retrieving the three-dimensional wind fileds by the combination of radial velocity from two Doppler radars. The continuity equation is employed in most dual Doppler radar studies, and in recent years, a variational technique has been applied to minimize a cost function, defined as the distance between the analysis and the observation, to yield optimal *u*, *v*, and *w* components. The variational method proposed by Gao et al.(1999) is a procedure that minimizes the cost function J and is defined as the sum of squared errors due to the misfit between observations and analyses subject to constrints. In this study, the constraints used in Protat et al. (1999) are adapted. When the analysis was performed, the simplified Shimizu and Maesaka(2006) cost function was used.

The study discovered that single-cells revealed a peak of core vorticity intensity after merging with pre-existing cells. The results of the height and time occurrence formation of peak core vorticity using pseudo-vorticity could distinguish the characteristic between single-cell and multicell due to its finest temporal and spatial resolution. The average formation height of single-cell for pair vorticity was 4.4 km calculated from the pseudo-vorticity method, compared with DDA, which showed the different heights of formation (3.8 km and 3.7 km) for positive and negative vorticity respectively. In addition, the pseudo-vorticity method indicated the average formation height of multicell was (3.8 km for positive vorticity, 2.7 km for negative vorticity), and (3.9 km for positive vorticity, 4.6 km for negative vorticity) based on DDA. From this finding, we could conclude that on average the single-cell showed the formation height of peak vorticity intensity at 4 km, and multicell slightly above 4.0 km. The results revealed the height of peak vorticity is mainly affected by the strength of the updraft. The frequent distribution of maximum updraft for multicell was revealed at a height of 4 km for intensity larger than 5 m s^{-1} and maximum downdraft with a strength greater than -1 m s^{-1} was observed at 1 km AGL. From our analysis, the average updraft velocities for the single-cell and multicell were 1.9 and 3.9 m s^{-1} respectively, and the average downdraft velocities were 0.7 and 1.4 m s^{-1}, respectively.

However, DDA vorticity showed similarities in time occurrence in single-cell, and differences in multicell. The time of peak was investigated related to the updraft strength and the height of the maximum updraft. The peak of these vorticities related to the convergence at the lower level influenced the updraft position, updraft strength, and wind motion. The convergence at a lower level also influenced the stretched of the vertical vortex tube and the amplification of vorticity intensity that occurred.

From the mechanism analysis, with the existence of the updraft, the horizontal vorticity would be tilted into the vertical vorticity. We found that the vertical vorticity mostly developed at the middle level for the new cells, parallel to the position of the updraft and generation of wind motion in the clouds. Due to the strength of the updraft and convergence, various heights were observed for the core vorticity of the new cells. The tilting of the vortex tube was influenced mostly at the middle level, similarly to the updraft position. These findings help us for a better understanding of the characteristics of single-cells that developed in multicell thunderstorms. In conclusion, the vertical vorticity is able to present the transition of cell merging process between single-cell and multicell, in terms of occurrence of peak, height, and time development of core vorticity. The transition signals help us to forecast the peak of rainfall after cells merged, and the threshold of single-cell merged discovered at the range of 0.002 s^{-1} to 0.004 s^{-1}. The mechanism analysis provided insight into the transition from single-cell to multicell development.

Acknowledgements

The authors express their sincere gratitude to Dr. S. Shimizu from the National Research Institute for Earth Science and Disaster Resilience (NIED), Tsukuba, Japan for the thoughtful discussions and for providing useful suggestions with the software developed regarding Dual Doppler radar analysis. This work was supported by JSPS KAKENHI Grant Numbers 15H05765, 20H02258. Fauziana Ahmad acknowledges the award of the Malaysian Public Service Department Training (HLP) scholarship allowing the research to be undertaken.

References

Bluestein, H. B., and M. H. Jain. (1985): Formation of Mesoscale Lines of Precipitation: Severe Squall Lines in Oklahoma during the Spring. J. Atmos. Sci., 42, pp. 1711–1732.

Boyer, C. H., and Dahl, J. M. L. (2020): The Mechanisms Responsible for Large Near-Surface Vertical Vorticity within Simulated Supercells and Quasi-Linear Storms. Monthly Weather Review 148, 10, pp. 4281-4297.

Dahl, J. M. L. (2017): Tilting of Horizontal Shear Vorticity and the Development of Updraft Rotation in Supercell Thunderstorms, Journal of the Atmospheric Sciences, 74(9), pp. 2997-3020.

E. Nakakita, R. Nishiwaki, H. Yamabe, and K. Yamaguchi. (2013): Research on the prognostic risk of baby cell for guerilla-heavy rainfall considering by vorticity with doppler velocity. The Journal of Japan Society of Civil Engineers, vol. 69, no. 4, pp. 325–330.

E. Nakakita, Sato, H., Nishiwaki, R., Yamabe, H., & Yamaguchi, K. (2017): Early Identification of Baby-Rain-Cell Aloft in a Severe Storm and Risk Projection for Urban Flash Flood. Advances in Meteorology, pp. (Article ID 5962356), pp. 1-15.

Franklin, C. N., Holland, G. J. and May, P. T.(2006): Mechanisms for the Generation of Mesoscale Vorticity Features in Tropical Cyclone Rainbands. Mon. Wea. Rev., 134(10), pp. 2649-2669.

Gao, j., M. Xue, A. Shapiro, and K. K. Droegemeier. (1999): A variational method for the analysis of three-dimensional wind fields from two Doppler radars. Mon. Wea. Rev., 127, pp. 2128–2142.

Geng, B., Fujiyoshi, Y. and Takeda, T. (1997): Evolution of a Multicell Thunderstorm in Association with Mid-Level Rear Inflow Enhanced by a Mid-Level Vortex in an Adjacent Thunderstorm, J. Meteor. Soc. Japan, 75, pp. 619-637.

Hirano, K., and M. Maki. (2010): Method of VIL calculation for X-band polarimetric radar and potential of VIL for nowcasting of localized severe rainfall -Case study of the Zoshigaya downpour, *SOLA*,6, pp. 89–92, doi:10.2151/sola.2010-023.

Kato, A., and M. Maki. (2009): Localized heavy rainfall near Zoshigaya, Tokyo, Japan on 5 August 2008 observed by X-band polarimetric radar: Preliminary analysis, *SOLA*, 5, pp.89-92, doi:10.2151/sola.2009–023.

Kim, D., Maki, M. and Shimizu, S. (2012): X-band Dual-Polarization Radar Observations of Precipitation Core Development and Structure in a Multicellular Storm over Zoshigaya, Japan, on August 5,2008. J. Meteor. Soc. Japan, 90(5), pp. 701-719.

Markowski, P. & Hannon, C. (2006): Multiple-Doppler Radar Observations of the Evolution of Vorticity Extrema in a Convective Boundary layer. *American Meteorological Society*, Volume 134, pp. 355-374.

Nishiwaki, N. et al. (2013): Behaviour and structure of convective clouds developing around a mountainous area observed by stereo photogrammetry and Ka-band and X-Band Radars: Case study of Northern Kanto, Japan. Journal of the Meteorological Society of Japan, 91(No.5), pp. 609-626.

Patrice Meunier, Stéphane Le Dizès, Thomas Leweke. (2005): Physics of vortex merging, Comptes Rendus Physique, Volume 6, Issues 4–5, pp. 431-450.

Peterson, R. E., Jr. (1984): A Triple-Doppler radar analysis of a discretely propagating multicell convective storm. J. Atmos. Sci., 41, pp. 2973–2990.

Protat, A. and Zawadzki, I. (1999): A Variational Method for Real-Time Retrieval of Three-Dimensional Wind Field from Multiple-Doppler Bistatic Radar Network Data. J. Atmos. Oceanic Technol., 16, pp. 432-449.

Ronald E. Rinehart. (2004): Radar for Meteorologists, Rinehart Publication, ISBN: 0-9658002-1-0.

Rotunno, R. (1981): On the Evolution of Thunderstorm Rotation. Mon. Wea. Rev., 109(3), pp. 577-586.

Shapiro, A. and Kogan, Y. L. (1994): On vortex formation in multicell convective clouds in a shear-free environment. Atmos. Res., 33(1-4), pp. 125-136.

Shimizu S, Maesaka T. (2006): Multiple Doppler radar Analysis using variational technique to retrieve three-dimensional wind field. Natl. Res. Inst. Earth Sci. Disast. Prevent. Res. Rep. **70**, pp.1–8.

Shimizu, S., H. Uyeda, Q. Moteki, and T. Maesaka. (2008): Structure and formation mechanism on the 24 May 2000 supercell-like storm developing in a moist environment over the Kanto Plain, Japan. Mon. Wea. Rev., 126, pp. 2389–2407.

Shimizu, S. (2012): Multiple Doppler Radar Analysis for Retrieving the Three-Dimensional Wind Field Within Thunderstorms. In: Doppler Radar Observations-Weather Radar, Wind Profiler, Ionospheric Radar, and Other Advanced Applications. Croatia: Intech, pp. 231-246.

Shusse, Y., Tsuboki, K., Geng, B., Minda, H., and Takeda, T. (2005): Structure and Evolution of Deeply Developed Convective Cells in a Long-Lived Cumulonimbus Cloud under a Weak Vertical Wind-Shear Condition, J. Meteor. Soc. Japan, 83, pp. 351-371.

Stalker, J. R. and Knupp, K. R. (2002): A Method to Identify Convective Cells within Multicell Thunderstorms from Multiple Doppler Radar Data. Mon. Wea. Rev., 130(1), pp. 188-195.

Weisman, M. L., and J. B. Klemp. (1982): The dependence of numerically-simulated convective storms on vertical wind shear and buoyancy. Mon. Wea. Rev., 110, pp. 504–520.

Weisman, M. L., and J. B. Klemp. (1984): The structure and classification of numerically simulated convective storms in directionally varying wind shears. Mon. Wea. Rev., 112, pp. 2479–2498.

Weisman M. L. and J. B. Klemp. (1986): Glossary of Meteorology. [Online] Available at: https://glossary.ametsoc.org/wiki/Bulk_richardson_number

(Received August 31, 2022)